VIP Batteries Very Important Paper

How to cite:
International Edition: doi.org/10.1002/anie.202104171
German Edition: doi.org/10.1002/ange.202104171

Can Aqueous Zinc–Air Batteries Work at Sub-Zero Temperatures?

Chang-Xin Zhao, Jia-Ning Liu, Nan Yao, Juan Wang, Ding Ren, Xiang Chen, Bo-Quan Li, and Qiang Zhang**

Abstract: *Efficient energy storage at low temperatures starves for competent battery techniques. Herein, inherent advantages of zinc–air batteries on low-temperature electrochemical energy storage are discovered. The electrode reactions are resistive against low temperatures to render feasible working zinc–air batteries under sub-zero temperatures. The relatively reduced ionic conductivity of electrolyte is identified as the main limiting factor, which can be addressed by employing a CsOH-based electrolyte through regulating the solvation structures. Accordingly, 500 cycles with a stable voltage gap of 0.8 V at 5.0 mA cm^{-2} is achieved at −10 °C. This work reveals the promising potential of zinc–air batteries for low-temperature electrochemical energy storage and inspires advanced battery systems under extreme working conditions.*

Rechargeable batteries constitute the core technique for the modern energy network.[1–3] Increasingly diversified human activities put forward requirements for rechargeable batteries towards various working conditions.[4,5] Especially, enabling rechargeable batteries at low temperatures is highly required for energy storage at high latitudes, high altitudes, abysmal sea, etc. Lithium-ion batteries (LIBs) have attracted worldwide attentions for low-temperature electrochemical energy storage. Nevertheless, LIBs suffer from limited capacity, poor rate performance, and short lifespan originated from high electrolyte freezing point and temperature-sensitive electrode kinetics.[6] Moreover, metallic lithium precipitation and dendrite growth at low temperatures induce performance degradation and even security hazards.[7] Therefore, new battery techniques are highly considered for efficient energy storage at low temperatures.[6,8]

Zinc-air batteries (ZABs) based on alkaline aqueous electrolyte employ metallic zinc and atmosphere oxygen as the anodic and cathodic active materials, respectively,[9–12] demonstrating great advantages of high theoretical energy density (1086 Wh kg^{-1}, including oxygen),[13] low cost,[14] source abundance,[15] inherent safety,[16] and potential to achieve high cycling current density and capacity.[17] More importantly, ZABs afford intrinsic advantages on low-temperature feasibility. On one hand, the high-concentrated aqueous electrolyte renders low freezing point according to the colligative properties. On the other hand, the ultralow and ultrahigh activation energies of the anodic and cathodic reactions result in insensitive electrode kinetics to varied temperatures based on the Arrhenius Equation. Therefore, ZABs are expected to demonstrate ideal resistance against low-temperature conditions.

Despite the theoretical advantages, the low-temperature performances of ZABs are seldomly investigated with only a few demonstrations of all-solid-state ZABs,[18] leaving the main bottleneck of low-temperature ZABs unclear. Herein, the low-temperature performances of ZABs are systematically investigated in terms of feasibility verification, bottleneck analysis, and promotion strategies. The feasible working temperature is identified as low as −40 °C and is rationalized based on fundamental physical chemistry. The relatively reduced ionic conductivity of the electrolyte is further identified as the main limiting factor, which is addressed by a CsOH-based electrolyte through regulating the solvation structures. This pioneer work reveals the unprecedented advantages of ZABs and inspires developing analogous batteries towards harsh working conditions.

The working feasibility of ZABs under low temperatures was experimentally evaluated using a conventional cell configuration with Pt/C + Ir/C as the cathodic electrocatalysts and aqueous electrolyte containing 6.0 M KOH and 0.20 M $Zn(OAc)_2$.[19,20] The low-temperature performances were firstly evaluated at −10 °C. As exhibited in Figure 1a, the linear sweep voltammetry (LSV) profile at −10 °C is comparable with that at 20 °C despite a bit higher polarization. A maximum output power density of 57.9 mW cm^{-2} was achieved, significantly larger than those of LIBs (generally lower than 10 mW cm^{-2}).[21,22] Acceptable rate performances at −10 °C were acquired to support galvanostatic discharge at 25 mA cm^{-2} (Figure 1b). Rechargeability is also confirmed at −10 °C with the voltage gaps of 1.0 and 1.5 V and lifespan of 165 and 65 cycles under current densities of 5.0 and 10 mA cm^{-2}, respectively (Figure 1c and d). To further extend the low temperature boundary of ZABs, LSV profiles were recorded down to −40 °C. Maximum output power densities of 29.9, 17.2, and 6.5 mW cm^{-2} were achieved at −20, −30, and −40 °C, respectively, manifesting the working potential of ZAB at extreme low temperatures (Figure 1e).

[*] C.-X. Zhao, J.-N. Liu, N. Yao, D. Ren, X. Chen, Prof. Q. Zhang
Beijing Key Laboratory of Green Chemical Reaction Engineering and Technology, Department of Chemical Engineering, Tsinghua University
Beijing 100084 (China)
E-mail: zhang-qiang@mails.tsinghua.edu.cn
J. Wang, Dr. B.-Q. Li
School of Materials Science & Engineering, Beijing Institute of Technology
Beijing 100081 (China)
and
Advanced Research Institute of Multidisciplinary Science, Beijing Institute of Technology
Beijing 100081 (China)
E-mail: libq@bit.edu.cn
Supporting information and the ORCID identification number(s) for the author(s) of this article can be found under: https://doi.org/10.1002/anie.202104171.

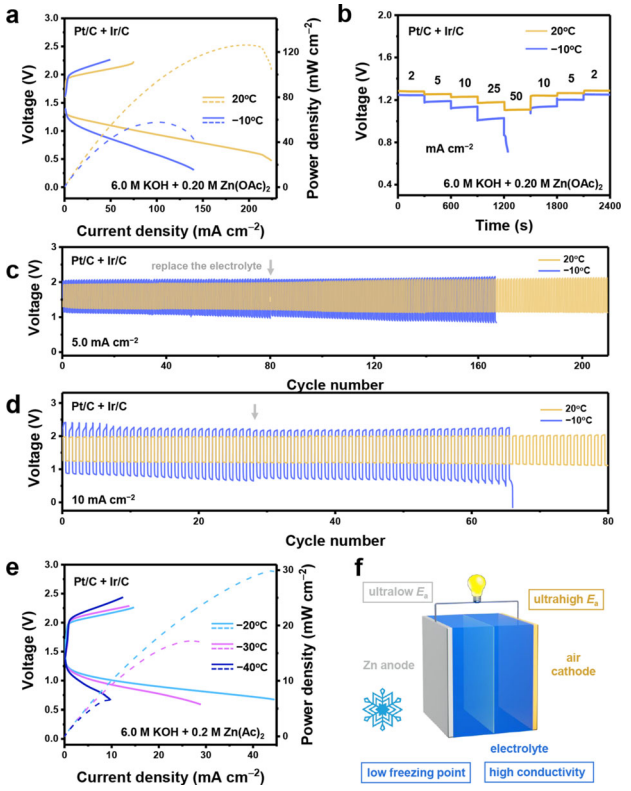

Figure 1. a) LSV profiles, b) rate performances, and galvanostatic cycling curves at c) 5.0 mA cm^{-2} and d) 10 mA cm^{-2} of ZABs at 20 and −10 °C. e) LSV profiles of ZABs at −20, −30, and −40 °C. f) Schematic diagram of the inherent advantages of ZABs for low-temperature energy storage.

The above results confirmed the working feasibility of ZAB at low temperatures, which is further rationalized based on the following physiochemistry analysis (Figure 1 f). Firstly, ZABs utilize highly concentrated alkaline aqueous electrolyte to ensure low freezing point of the electrolyte according to the colligative properties, where the liquid electrolyte supports efficient electrochemical reactions.[23] Secondly, the electromigration capability of OH^- is ultrahigh under the unique hopping mechanism ($\lambda_{0,\ OH^-} = 0.0198\ S\,m^2\,mol^{-1}$). Consequently, the conductivity of alkaline aqueous electrolyte is generally larger than organic electrolyte especially at low temperatures. Thirdly, the kinetics of the zinc anode is fast enough with an ultralow activation energy (E_a)[24,25] while the kinetics of the oxygen cathode (oxygen evolution and reduction reactions, OER/ORR) is very sluggish to render an ultrahigh E_a.[26,27] Fortunately, reactions with ultralow or ultrahigh E_a demonstrate relative insensitivity against changeable temperatures to afford no significant kinetic decline under low temperatures (see Figure S1 for detailed discussion). The above properties account for the inherent advantages of ZABs to satisfy low-temperature electrochemical energy storage.

Despite the low-temperature working feasibility from experimental and theoretical perspectives, the decline in electrochemical performances at low temperature is still detectable. In order to determine the main bottleneck and rationally improve the low-temperature performances, the low-temperature responses of the electrolyte, cathode, and anode are, respectively evaluated as follows:

(1) Electrolyte freezing. To measure the freezing point of the electrolyte, liquid-solid phase diagram was plotted (Figure S2). Complying with the colligative property, the freezing point reduces with the increase of the solute concentration. A freezing point lower than −44 °C was achieved in the 6.0 M KOH electrolyte, denying electrolyte freezing as the main bottleneck.

(2) Cathodic reaction. To evaluate influence of low temperature on the cathodic reactions, ORR/OER activity of the Pt/C + Ir/C electrocatalyst was investigated utilizing rotating ring-disc electrodes. As is exhibited in Figure 2 a and b, low temperature has little effect on both ORR and OER with only 10 mV decrease of the ORR half-wave potential and 20 mV increase of the OER overpotential to achieve 10 mA cm^{-2}, significantly lower than the increased polarization of corresponding ZABs. The Tafel slopes (Figure S3) and electrochemical impedance spectroscopy results (EIS, insert in Figure 2 a and b) are also comparable at different temperatures. Additionally, the ORR limiting current density and the ORR electron transfer number are unaffected under lower temperatures (Figure S4), manifesting little effect on oxygen mass transfer or the selective 4 e$^-$ reduction pathway.[28]

(3) Anodic reaction. Zn-Zn symmetry cells were evaluated to determine the influence of anodic kinetics. The cyclic

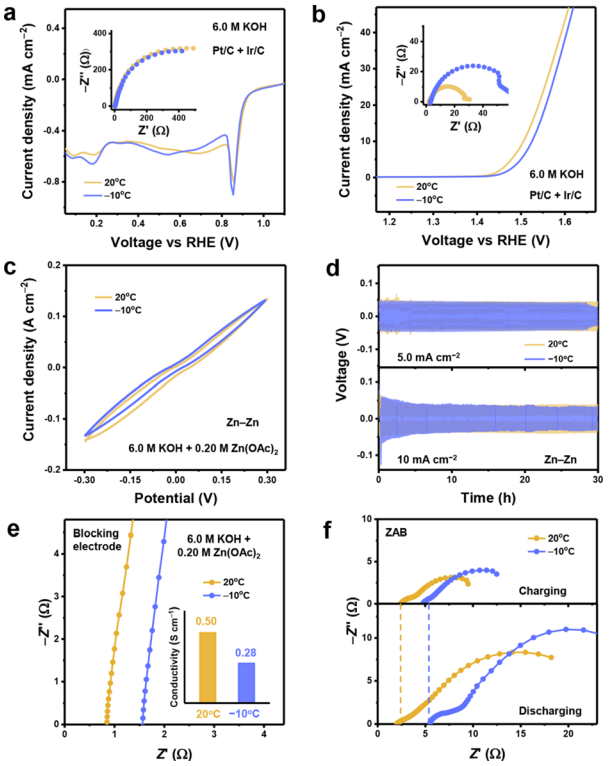

Figure 2. a) ORR and b) OER LSV curves of the Pt/C + Ir/C electrocatalyst in KOH-based electrolyte at 20 and −10 °C. The inserts are corresponding EIS spectra. c) CV profiles and d) galvanostatic cycling curves of Zn–Zn symmetric cells at 20 and −10 °C. e) EIS spectra of the blocking electrodes. The insert is corresponding conductivity. f) EIS spectra of ZABs at 20 and −10 °C.

voltammetry (CV) profiles at −10 °C is almost identical to that at 20 °C with both curves indicating fast anodic kinetics (Figure 2c and Figure S5). Long-term cycling tests also afford similar results with equally stable charge/discharge voltage gaps of 80 mV (at 5.0 mA cm^{-2}) and 100 mV (at 10 mA cm^{-2}) at different temperatures (Figure 2d). Therefore, the intrinsic fast kinetics of the zinc anode and insensitivity against varied temperatures dispel the suspicion from the anode side.

(4) Electrolyte conductivity. Notably, the electrolyte conductivity at −10 °C is almost reduced by half using the blocking electrode method (Figure 2e). Further quantitative measurements indicate the electrolyte conductivity is 0.50 and 0.28 S cm^{-1} at 20 °C and −10 °C, respectively. The reduced conductivity leads to increased battery internal resistance of ca. 3 Ω and nonnegligible ohmic polarization in agreement with the LSV profiles of ZABs (Figure 2f). In conclusion, reduced electrolyte conductivity and consequent increased resistance serve as the main limiting factor of low-temperature ZABs.

Based on the above analysis, promoting the electrolyte conductivity is expected to realize performance promotion of low-temperature ZABs. Concretely, the reduce of electromigration capability is mainly attributed to strong interactions between OH^- and alkali cations. Therefore, regulating the solvation structure by using different alkali cations can modulate the interactions to increase electrolyte conductivity under low temperatures.[29] A series of alkaline electrolyte containing 6.0 M MOH and 0.20 M $Zn(OAc)_2$ (M = Li, Na, K, Rb, Cs; 5.0 M LiOH, considering its limited solubility) were configured (Figure 3a). Except for the LiOH-based electrolyte, all the electrolytes remain liquid-phased even at −30 °C (Figure 3a and S6). Despite the reduced electrolyte conductivity with lower temperatures, the conductivity of the electrolytes follows a sequence of Li < Na < K < Rb < Cs within the temperature range, suggesting CsOH-based electrolyte with potential to promote low-temperature ZABs (Figure 3b).

Molecular dynamics (MD) simulations of the electrolytes were further conducted to afford atomic insights (Figure 3c). The CsOH-based electrolyte delivers the largest mean square displacements ($\langle|r(t)-r(0)|^2\rangle$, MSDs) of both M^+ and OH^- at −10 °C (Figure 3d and e) to manifest its largest ionic diffusion coefficient (D) according to the Einstein's diffusion law ($\lim_{(t\to\infty)}\langle|r(t)-r(0)|^2\rangle = 6Dt$). The largest diffusion coefficient corresponds to the largest ion mobility (u) and electrolyte conductivity according to the Einstein-Smoluchowski equation.[30] The enhancement on electrolyte conductivity is assigned to the regulated solvation structure. Specifically, with the increase of the atomic number, the ionic radius increases and the positive charge density gets dispersed, leading to weakened Coulomb force between alkali metal cations and OH^-. Monitored by the radial distribution functions g(r), the cation with larger atomic number exhibits weaker interactions with OH^- to render a sparse solvation structure (Figure 3f).[31,32] The weakly solvating electrolyte affords more free ions to support electromigration (Figure 3g and S7). Meanwhile, the absence of cations in the anion solvation

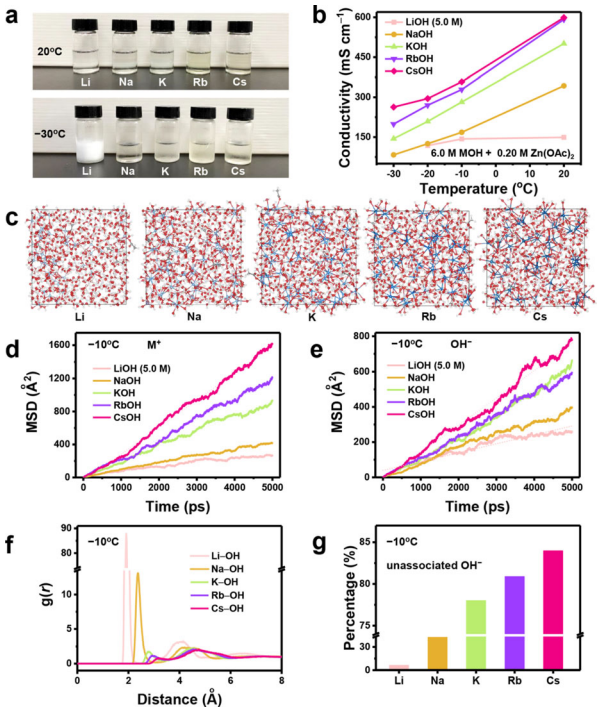

Figure 3. a) Optical images and b) conductivity of the electrolytes with various alkali metal cations. c) Snapshots of the MD simulation boxes of various electrolytes at −10 °C. Colors for different elements: H white, O red, C gray, Zn purple, alkali metal blue. Diffusion coefficient simulations of d) M^+ and e) OH^- based on MSD analysis at −10 °C. f) M-OH radical distribution function and g) percentage of unassociated OH^- in different electrolytes at −10 °C.

structure ensures necessary interactions (hydrogen bond) between hydroxide anions and water molecules to facilitate the hopping conduction process. Both the factors contribute to the apparent high conductivity of the CsOH-based electrolyte especially under low temperatures.

Utilizing the high-conductive CsOH-based electrolyte is expected to achieve promoted low-temperature performances. According to the LSV profiles in Figure 4a, the CsOH-based electrolyte renders ZABs with lower polarization and almost doubled maximum discharge power density (57.9 and 99.3 mW cm^{-2} for the KOH and CsOH-based electrolytes, respectively). Promoted rate performances were also achieved (Figure 4b). Specifically, the discharging voltage increased with 11, 25, 51, and 109 mV under current densities of 2, 5, 10, and 25 mA cm^{-2}, respectively. The CsOH-based electrolyte also affords the ZABs with long-cycling stability. Under the cycling current densities of 5.0 and 10 mA cm^{-2}, not only was the voltage gap, respectively reduced by 0.2 and 0.3 V, but also satisfactory lifespan of 500 and 120 cycles was achieved (Figure 4c and S8). The CsOH-based electrolyte also boosts the performances under severe cold conditions of −20 °C (Figure S9, S10, and S11).

The achieved working temperature of −20 °C can cover 99.6 % of the population on earth to satisfy outdoor energy storage in winter (Figure 4d and S12). To intuitively exemplify the feasibility of ZABs for low-temperature outdoor applications, a mobile power based on the ZABs with the CsOH-based electrolyte was fabricated (Figure S13). For

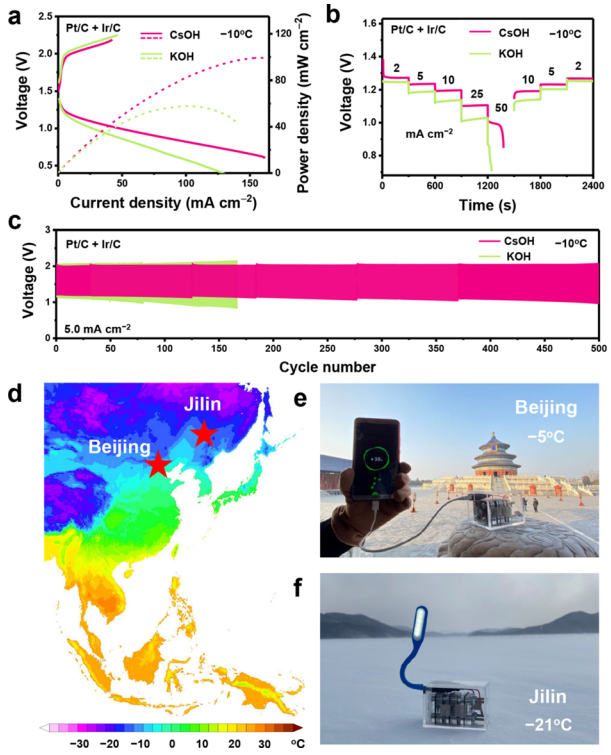

Figure 4. a) LSV profiles, b) rate performances, and c) galvanostatic cycling curves at 5.0 mA cm^{-2} of the CsOH-based electrolyte at −10 °C. d) Average air temperature in January from 2010 to 2019. e) Charging a mobile phone in the Temple of Heaven, Beijing and f) powering a LED light on the snowy frozen Songhua Lake in Jilin utilizing the mobile power based on ZABs.

outdoor winter occasions, the assembled mobile power is capable to charge a mobile phone at −5 °C in Beijing (Figure 4e) and to power a 1.2 W light-emitting diode (LED) light in Jilin Province, China at −21 °C (Figure 4f). These results demonstrate great potential of ZABs for low-temperature energy storage in the near future.

In conclusion, the low-temperature performances of ZABs are systematically investigated. Theoretical and experimental analyses validate the inherent advantages for low-temperature ZABs regarding high-concentration aqueous electrolyte and electrode kinetics insensitive against varied temperatures. Furthermore, low electrolyte conductivity is identified as the main limitation, which is addressed by a novel CsOH-based electrolyte through regulating the solvation structures. This work reveals the great potential of low-temperature ZABs and inspires developing advanced battery systems working at extreme conditions.

Acknowledgements

This work was supported by National Key Research and Development Program (2016YFA0200102), Natural Scientific Foundation of China (21825501), and Tsinghua University Initiative Scientific Research Program. The authors acknowledged the support from Tsinghua National Laboratory for Information Science and Technology for theoretical simulations. We thank Dr. Jia Yu and Prof. Jia-Qi Huang for helpful discussion.

Conflict of interest

The authors declare no conflict of interest.

Keywords: electrolyte · low temperature · solvation structure · zinc–air batteries

[1] H. B. Yang, J. Miao, S.-F. Hung, J. Chen, H. B. Tao, X. Wang, L. Zhang, R. Chen, J. Gao, H. M. Chen, L. Dai, B. Liu, *Sci. Adv.* **2016**, *2*, e1501122.
[2] P. K. Nayak, L. Yang, W. Brehm, P. Adelhelm, *Angew. Chem. Int. Ed.* **2018**, *57*, 102–120; *Angew. Chem.* **2018**, *130*, 106–126.
[3] Z. Du, X. Chen, W. Hu, C. Chuang, S. Xie, A. Hu, W. Yan, X. Kong, X. Wu, H. Ji, L.-J. Wan, *J. Am. Chem. Soc.* **2019**, *141*, 3977–3985.
[4] J. B. Goodenough, *Energy Storage Mater.* **2015**, *1*, 158–161.
[5] Y. Liang, C.-Z. Zhao, H. Yuan, Y. Chen, W. Zhang, J.-Q. Huang, D. Yu, Y. Liu, M.-M. Titirici, Y.-L. Chueh, H. Yu, Q. Zhang, *InfoMat* **2019**, *1*, 6–32.
[6] J. Hou, M. Yang, D. Wang, J. Zhang, *Adv. Energy Mater.* **2020**, *10*, 1904152.
[7] Q. Q. Liu, D. J. Xiong, R. Petibon, C. Y. Du, J. R. Dahn, *J. Electrochem. Soc.* **2016**, *163*, A3010–A3015.
[8] T. Sun, H. Du, S. Zheng, J. Shi, Z. Tao, *Adv. Funct. Mater.* **2021**, *31*, 2010127.
[9] Y.-P. Deng, Y. Jiang, R. Liang, S.-J. Zhang, D. Luo, Y. Hu, X. Wang, J.-T. Li, A. Yu, Z. Chen, *Nat. Commun.* **2020**, *11*, 1952.
[10] W. Sun, F. Wang, B. Zhang, M. Zhang, V. Kuepers, X. Ji, C. Theile, P. Bieker, K. Xu, C. Wang, M. Winter, *Science* **2021**, *371*, 46–51.
[11] H.-F. Wang, Q. Xu, *Matter* **2019**, *1*, 565–595.
[12] F. Meng, H. Zhong, J. Yan, X. Zhang, *Nano Res.* **2017**, *10*, 4436–4447.
[13] F. Meng, H. Zhong, D. Bao, J. Yan, X. Zhang, *J. Am. Chem. Soc.* **2016**, *138*, 10226–10231.
[14] Y. Zhao, Y. Zhu, X. Zhang, *InfoMat* **2020**, *2*, 237–260.
[15] J. Fu, Z. P. Cano, M. G. Park, A. Yu, M. Fowler, Z. Chen, *Adv. Mater.* **2017**, *29*, 1604685.
[16] H. Sun, M. Wang, S. Zhang, S. Liu, X. Shen, T. Qian, X. Niu, J. Xiong, C. Yan, *Adv. Funct. Mater.* **2021**, *31*, 2006533.
[17] C.-X. Zhao, J.-N. Liu, B.-Q. Li, D. Ren, X. Chen, J. Yu, Q. Zhang, *Adv. Funct. Mater.* **2020**, *30*, 2003619.
[18] L. An, B. Huang, Y. Zhang, R. Wang, N. Zhang, T. Dai, P. Xi, C.-H. Yan, *Angew. Chem. Int. Ed.* **2019**, *58*, 9459–9463; *Angew. Chem.* **2019**, *131*, 9559–9563.
[19] G. Li, X. Wang, J. Fu, J. Li, M. G. Park, Y. Zhang, G. Lui, Z. Chen, *Angew. Chem. Int. Ed.* **2016**, *55*, 4977–4982; *Angew. Chem.* **2016**, *128*, 5061–5066.
[20] J. Wang, J. Liu, Z. Du, Z. Li, *J. Energy Chem.* **2021**, *54*, 770–785.
[21] J. Shi, N. Ehteshami, J. Ma, H. Zhang, H. Liu, X. Zhang, J. Li, E. Paillard, *J. Power Sources* **2019**, *429*, 67–74.
[22] A. Tron, S. Jeong, Y. D. Park, J. Mun, *ACS Sustainable Chem. Eng.* **2019**, *7*, 14531–14538.
[23] J. Yu, B.-Q. Li, C.-X. Zhao, J.-N. Liu, Q. Zhang, *Adv. Mater.* **2020**, *32*, 1908488.
[24] G. Fang, J. Zhou, A. Pan, S. Liang, *ACS Energy Lett.* **2018**, *3*, 2480–2501.
[25] L. Cao, D. Li, E. Hu, J. Xu, T. Deng, L. Ma, Y. Wang, X.-Q. Yang, C. Wang, *J. Am. Chem. Soc.* **2020**, *142*, 21404–21409.

[26] J. Sun, S. E. Lowe, L. Zhang, Y. Wang, K. Pang, Y. Wang, Y. Zhong, P. Liu, K. Zhao, Z. Tang, H. Zhao, *Angew. Chem. Int. Ed.* **2018**, *57*, 16511 – 16515; *Angew. Chem.* **2018**, *130*, 16749 – 16753.
[27] C. Tang, H.-F. Wang, X. Chen, B.-Q. Li, T.-Z. Hou, B. Zhang, Q. Zhang, M.-M. Titirici, F. Wie, *Adv. Mater.* **2016**, *28*, 16749 – 16753.
[28] G. Zhong, S. Xu, L. Liu, C. Z. Zheng, J. Dou, F. Wang, X. Fu, W. Liao, H. Wang, *ChemElectroChem* **2020**, *7*, 1107 – 1114.
[29] H. M. Lee, P. Tarakeshwar, J. Park, M. R. Kolaski, Y. J. Yoon, H. B. Yi, W. Y. Kim, K. S. Kim, *J. Phys. Chem. A* **2004**, *108*, 2949 – 2958.
[30] J. R. Sangoro, A. Serghei, S. Naumov, P. Galvosas, J. Kaerger, C. Wespe, F. Bordusa, F. Kremer, *Phys. Rev. E* **2008**, *77*, 051202.
[31] Q. Zou, Z. Liang, G.-Y. Du, C.-Y. Liu, E. Y. Li, Y.-C. Lu, *J. Am. Chem. Soc.* **2018**, *140*, 10740 – 10748.
[32] S. I. Lukyanov, Z. S. Zidi, S. V. Shevkunov, *Chem. Phys.* **2007**, *332*, 188 – 202.

Manuscript received: March 24, 2021
Accepted manuscript online: May 3, 2021
Version of record online: ■■ ■■, ■■■■

Communications

Batteries

C.-X. Zhao, J.-N. Liu, N. Yao, J. Wang, D. Ren, X. Chen, B.-Q. Li,* Q. Zhang* _____ ■■■■–■■■■

Can Aqueous Zinc–Air Batteries Work at Sub-Zero Temperatures?

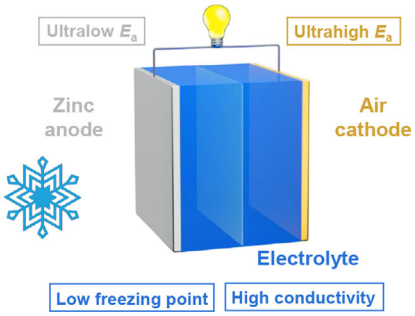

The low-temperature performances of zinc–air batteries are systematically investigated from both theoretical and experimental aspects in terms of feasibility verification, bottleneck analysis, and promotion strategies.